JACS
JOURNAL OF THE AMERICAN CHEMICAL SOCIETY

Article

pubs.acs.org/JACS

NO Disproportionation at a Mononuclear Site-Isolated Fe^{2+} Center in Fe^{2+}-MOF-5

Carl K. Brozek,[†] Jeffrey T. Miller,[‡,⊥] Sebastian A. Stoian,[§] and Mircea Dincă*[,†]

[†]Department of Chemistry, Massachusetts Institute of Technology, 77 Massachusetts Avenue, Cambridge, Massachusetts 02139, United States

[‡]Chemical Sciences and Engineering Division, Argonne National Laboratory, Lemont, Illinois 60439, United States

[§]National High Magnetic Field Laboratory, Florida State University, Tallahassee, Florida 32310, United States

[⊥]Department of Chemical Engineering, Purdue University, 480 Stadium Mall Dr., West Lafayette, Indiana 47907, United States

Supporting Information

ABSTRACT: The weak-field ligand environments at the metal nodes of metal−organic frameworks (MOFs) mimic the electronic environment of metalloenzyme active sites, but little is known about the reactivity of MOF nodes toward small molecules of biological relevance. Here, we report that the ferrous ions in Fe^{2+}-exchanged MOF-5 disproportionate nitric oxide to produce nitrous oxide and a ferric nitrito complex. Although mechanistic studies of N−N bond forming transformations often invoke a hyponitrite species, as in nitric oxide reductase and NO_x reduction catalysis, little is known about this intermediate in its monoanionic state. Together with the first report of N−N coupling between NO molecules in a MOF, we present evidence for a species that is consistent with a ferric hyponitrite radical, whose isolation is enabled by the spatial constraints of the MOF matrix.

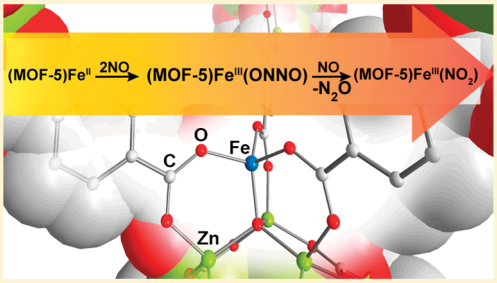

INTRODUCTION

The chemical transformation of nitric oxide mediated by transition metal ions underlies crucial processes in both nature and in environmental protection. NO is a chief component of N_xO_y species that contaminate the atmosphere[1] and is targeted in N_xO_y reduction catalysis.[2,3] Immune response, blood pressure control, and neurotransmission require the generation and decay of nitric oxide[4] by metal-containing molecules such as the heme enzyme known as soluble guanylyl cyclase (sGC).[5] Although NO transformations in these biological examples occur under homogeneous conditions, they are mediated by active sites and clusters supported by weak-field ligands such as carboxylates and imidazolates. These functionalities are identical to those found in most metal−organic frameworks (MOFs), making the latter intriguing candidates for functional biomimetic studies.

With mounting recent evidence from us and others that MOF nodes can undergo redox transformations,[6−11] we have begun exploring the chemistry of biologically relevant small molecules by conceiving of the metal nodes as electronically isolated molecules. Here, we show that Fe^{2+}-substituted $Zn_4O(terephthalate)_3$ (Fe^{2+}-MOF-5) mediates the disproportionation of NO with formation of N_2O. In this material, the key N−N coupling step required for the formation of N_2O from NO involves a single Fe atom, in contrast with natural systems that evolve N_2O, such as nitric oxide reductase (NOR), where bimetallic FeFe centers are required for the formation of the N−N bond[12,13] through a putative hyponitrite species.[14−17] Additional investigations into the mechanism of this reaction allowed us to identify a species that is most consistent with a ferric hyponitrite radical. To our knowledge, these results are the first to provide experimental evidence of a monoanionic hyponitrite radical intermediate implicated in the formation of a N−N bond, and constitute the first example of a MOF promoting NO reactivity of any kind. Although the disproportionation of 3 equiv of NO in Fe^{2+}-MOF-5 is a different transformation than what occurs in NOR and deNO$_x$ catalysts, this study highlights the potential of MOFs as useful platforms for studying the general features that underlie transformations of small molecules by isolating uncommon intermediates in biologically relevant ligand fields.

RESULTS

Early evidence that Fe^{2+}-MOF-5, shown in Figure 1, displays a unique interaction with NO originated in our previous report of an activated {FeNO}^{7} complex with an NO stretching frequency of 1793 cm^{-1}, much lower than those reported for NO interacting with other MOFs.[9] We attributed this strong activation of NO to the iron sites in the original Fe^{2+}-MOF-5 being in a high spin configuration. Indeed, magnetic susceptibility measurements confirm that Fe^{2+}-MOF-5 features isolated $S = 2$ ferrous ions (Supporting Information Figure S1). At room temperature, the material displays a μ_{eff} of 5.07 μ_B,

Received: April 17, 2015
Published: May 19, 2015

DOI: 10.1021/jacs.5b03761
J. Am. Chem. Soc. 2015, 137, 7495−7501

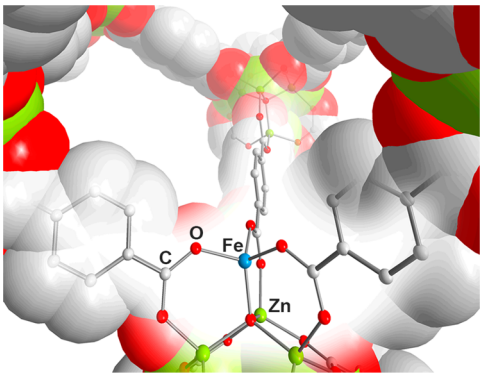

Figure 1. Illustration of the secondary building unit of MOF-5 where Fe^{2+} substitutes one of the Zn^{2+} ions to furnish Fe^{2+}-MOF-5.

near the expected 4.90 μ_B. Our initial evidence that Fe^{2+}-MOF-5 promotes further reactivity with NO came from observing the spectral features of the $\{FeNO\}^7$ species decay over the course of several minutes. Whereas treatment of an evacuated sample of yellow Fe^{2+}-MOF-5 with NO at room temperature induced a color change to black, corresponding to the formation of iron nitrosyl $\{FeNO\}^7$ (**B**, in Scheme 1), continued exposure to NO

Scheme 1

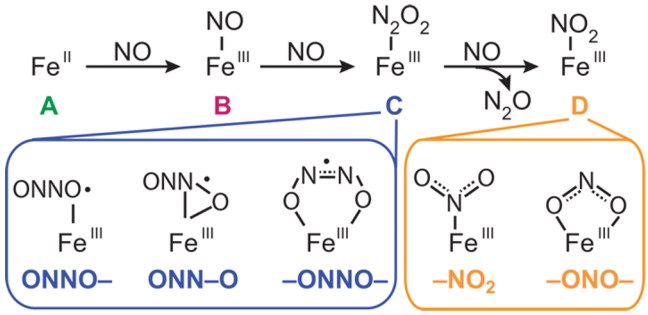

caused the black crystals to gradually turn bright orange. The decay of the black $\{FeNO\}^7$ adduct and the formation of the new orange product was followed by in situ diffuse reflectance UV–vis-NIR spectroscopy, which evidenced the decay of the broad ligand-to-metal NO(π^*) → d charge transfer band at 476 nm present in **B** (Supporting Information Figure S2).

In situ diffuse reflectance infrared Fourier transform spectroscopy (DRIFTS) provided further clues for the decomposition of **B**. The strong band centered at 1793 cm^{-1}, attributed to the N–O stretch (ν_{NO}) of the nitrosyl group in **B**, decreased in intensity over 10 min (Figure 2), with concomitant emergence of new bands at 1178 and 868 cm^{-1} arising from what we label as species **C**. Surprisingly, the new bands from **C** reached their maximum intensity after 30 min and then receded over the course of another 30 min, leaving a new set of resonant features at 1220, 1000, and 797 cm^{-1}, evidencing the formation of a yet new species, **D**. Representative spectra from the time evolution DRIFTS analysis of steps **B** → **C** and **C** → **D** are shown in Figure 2. For completeness, all spectra are shown in Supporting Information Figure S3. The IR frequencies describing the **A** → **B** → **C** → **D** transformation are summarized in Table 1. Although species **C** was observed only transiently under excess NO, we were able to isolate it by evacuating our in situ DRIFTS cell immediately before the spectral features from species **D** began to emerge. Species **C** is stable under vacuum or N_2, but produces species **D** in less than a minute after exposure to NO. Analysis of the final material by powder X-ray diffraction (PXRD) confirmed that the crystallinity is retained throughout the entire transformation (Supporting Information Figure S4). Moreover, a Brunauer–Emmett–Teller (BET) analysis of an N_2 adsorption isotherm measured at 77 K for the final species, **D**, revealed a surface area of 3218 m^2/g, in agreement with that reported for MOF-5 itself.[18] Analysis of the adsorption data using density functional theory[19] revealed a narrow pore size distribution centered at 12.68 Å. This value is similar to the 11.79 Å we measured for the Fe-MOF-5 starting material and comparable to the diameter observed by X-ray crystallography. Therefore, the PXRD and N_2 isotherm analyses confirmed that no part of the material decomposed during the transformation (Supporting Information Figure S5).

To investigate whether any gases are evolved during the **B** → **C** → **D** reaction sequence, we sampled the headspace of the batch reactor used for in situ DRIFTS by real-time gas analysis and quadrupole mass spectrometry (RGA-MS). Because signal spikes can be artifacts of monitoring MS in flow, we altered the setup to detect N_2O with greater certainty: once the full **B** → **D** sequence was completed after about 1 h, as indicated by DRIFTS, we cooled the reactor to −150 °C and applied vacuum so that frozen N_2O would remain in the chamber, but excess NO and N_2, expected to remain in the gaseous phase at this temperature, would not. The reactor was warmed to room temperature and attached in line to the mass spectrometer with a flow of He/Ar. After establishing a stable baseline for signals at 30 and 44 amu, corresponding to NO and N_2O, respectively, the reactor was opened to the flow setup for detection. As shown in Supporting Information Figure S6, a signal appeared for N_2O and took 132 s to reach baseline levels, whereas the detection of NO remained unperturbed.

With evidence that N_2O is evolved as part of the sequential **B** → **C** → **D** transformation, we employed X-ray absorption spectroscopy (XAS) to probe the oxidation states and coordination environments of the iron sites in **C** and **D**, since they were expected to change during these transformations. Comparing the K-edge spectrum of pristine Fe^{2+}-MOF-5 to those of species **C** and **D** revealed a shift to higher energy in both the pre-edge (1s → 3d) and rising edge (1s → 2p) features (Figure 3), suggesting that the iron sites undergo one e^- oxidation to Fe^{3+} relative to species **A** (Fe^{2+}-MOF-5), a ferrous compound. By analyzing the difference spectrum from the XAS data, the extended X-ray absorption fine structure (EXAFS) regions indicate that both **C** and **D** contain additional ligands (Figure 3). These new scattering pairs were fit to a coordination number of 0.9 at a distance of 1.98(2) Å for **C** and 1.2 at a distance of 2.08(2) Å for **D**.

The zero-field ^{57}Fe Mössbauer spectrum recorded at 70 K for species **D** exhibits two broad resonances that can be described using an isomer shift δ = 0.5(1) mm/s and a quadrupole splitting ΔE_Q = 0.75(4) mm/s (see Figure S7). These values are typical of high-spin ferric ions. The observed broadening originates from the incidence of unresolved magnetic hyperfine splitting, as is typical of Kramers systems. These observations confirm that all iron sites in **D** are oxidized to mononuclear, high-spin Fe(III) ions. In contrast, the zero-field spectrum recorded at 4.2 K for the starting material A consists of a quadrupole doublet with resonances that are much narrower and are characterized by δ = 1.15(2) mm/s and ΔE_Q = 3.03 (1). These values are typical of high-spin Fe(II) ions.[20] Finally,

DOI: 10.1021/jacs.5b03761
J. Am. Chem. Soc. 2015, 137, 7495–7501

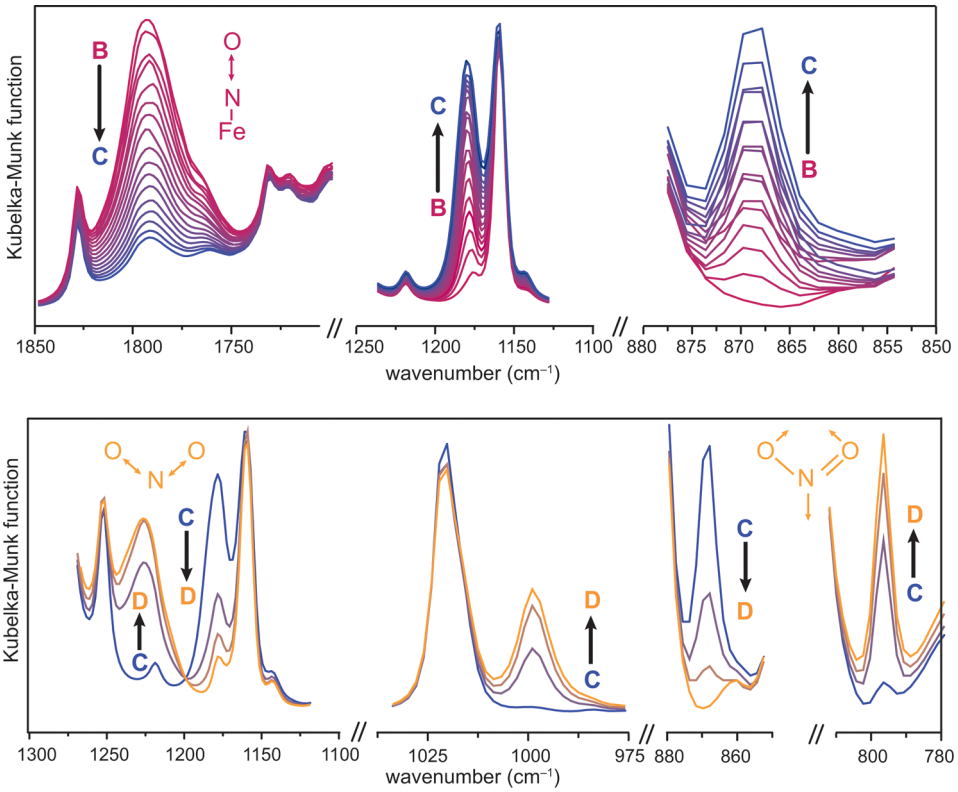

Figure 2. In situ DRIFTS collected on Fe-MOF-5 during reaction with NO. Species **B** is shown in pink, species **C** in blue, and species **D** in gold. IR-active modes are depicted in the same color as the corresponding spectral feature.

Table 1. Measured DRIFTS Bands for Species B–D in cm^{-1} that Appear after Treating Fe-MOF-5 with NO[a]

	natural abundance NO	^{15}NO
B	1793 (s)	1760 (s)
C	1178 (m), 868 (w)	1155 (m), 863 (w)
D	1220 (m), 1000 (m), 797 (w)	1193 (m), 1000 (m), 776 (w)

[a]Intensities are indicated in parentheses.

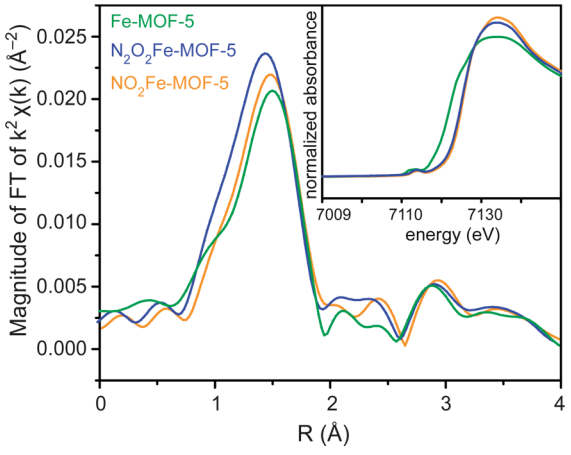

Figure 3. X-ray absorption spectra of Fe-MOF-5 (green), species **C** (blue), and species **D** (gold). Comparative R-space EXAFS are shown in large format with comparative XANES shown as an inset.

the X-band electron paramagnetic resonance (EPR) spectra recorded at 77 K for species C and D showed broad resonances centered at g_{iso} = 4.3, common for mononuclear, high-spin ferric ions (see Supporting Information Figures S8 and S9).[21]

To verify our mass spectrometry assignment of N_2O evolution as well as the vibrational spectral features of our DRIFTS data, we repeated these experiments using ^{15}NO. As shown in Figure 4, all except one of the peaks that evolve during the **B** → **C** → **D** sequence are sensitive to isotopic substitution, indicating that they involve the transformation of N_xO_y species. The ν_{NO} of **B** shifts from 1793 to 1760 cm^{-1}, which is close to the difference of 32 cm^{-1} expected from the harmonic oscillator approximation. When **C** is formed from ^{15}NO, peaks grow in at 1155 and 863 cm^{-1}. These are shifted by 25 and 5 cm^{-1} relative to those observed with natural abundance NO, but deviate from shifts of 21 and 16 cm^{-1} predicted by the harmonic oscillator approximation. As species **D** is formed from ^{15}NO, features appear at 1193 and 776 cm^{-1} that are shifted by 33 and 20 cm^{-1}, respectively. These shifts also deviate from the harmonic oscillator predictions of 22 and 14 cm^{-1} for pure N–O stretches. The transient DRIFTS spectra under ^{15}NO are shown in Supporting Information Figure S10, and the values are summarized in Table 1. Interestingly, the mode at 1000 cm^{-1}, which is not present in Fe^{2+}-MOF-5, is not sensitive to isotopic substitution. Finally, sampling the headspace by using the same procedure as for natural abundance NO revealed a prominent mass fragment at 46 amu, as expected for doubly ^{15}N-labeled $(^{15}N)_2O$, confirming that both expected products from NO disproportionation are present at the end of the reaction sequence (Supporting Information Figure S11).

DISCUSSION

Taken together, the observations described above are consistent with the reaction sequence shown in Scheme 1. Because the transformation occurs over the span of an hour, by

DOI: 10.1021/jacs.5b03761
J. Am. Chem. Soc. 2015, 137, 7495–7501

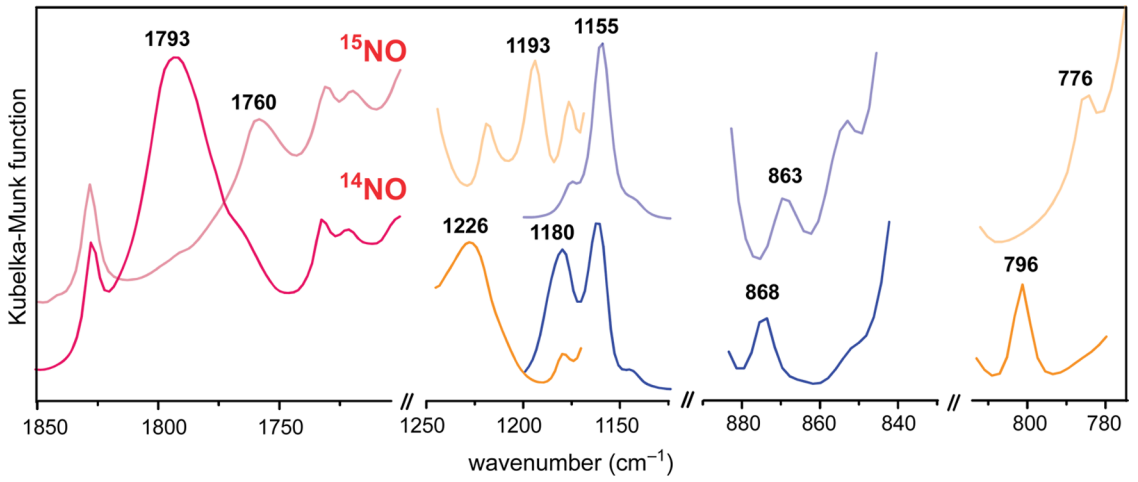

Figure 4. Comparative DRIFTS features for species **B** (pink), species **C** (blue), and species **D** (gold) shown when using natural abundance NO (dark traces) and ^{15}NO (light traces).

assuming pseudo-first-order dependence on Fe^{2+} sites, we estimate that $k < 0.01$ s^{-1} for the rate-determining step. An informative comparison can be drawn from a recent report on the isolation of an $\{FeNO\}^7$ species within the material known as Fe-MOF-74.[11] In this material, the $\{FeNO\}^7$ species does not proceed onto further disproportionation, perhaps because the $\{FeNO\}^7$ lack open coordination sites. Scheme 1 likely occurs in Fe-MOF-5 because the ferrous sites begin with four-coordinate geometry. The frequencies of the isotopically sensitive normal modes are consistent with the N−O IR-active modes of various N_xO_y species, such as NO_2^- or $N_2O_2^{m-}$, where m = 1 or 2, which are expected to result as products or intermediates from nitric oxide disproportionation.[22] Because the band that emerges with **D** at 1000 cm^{-1} is not susceptible to isotopic substitution, it likely originates from a new lattice mode that is induced by geometric distortions of the iron sites. Of the three possible binding modes of NO_2^- to the ferric centers, the EXAFS data of **D** are best fitted to a model where the NO_2^- is bound to Fe^{3+}-MOF-5 in η^1 fashion. The distance of 2.08(2) Å is suggestive of either a nitrito species,[23−25] or a nitro (i.e., N-bound) species.[26−28] Although nitrito species with η^2 coordination also display distances near the value we observed for **D**,[24,29,30] EXAFS analysis identified only one scatterer near the Fe atom, rather than two. The DRIFTS feature at 797 cm^{-1} observed for species **D** is similar to reported values for δ_{ONO}, while the band at 1220 cm^{-1} is reasonable for ν_{NO} for N−O species with bond orders between one and two, as found in nitrite.[31]

A more complicated assignment befits species **C**. Initially, the conversion from **C** to **D** seemed to be an isomerization between coordination modes of NO_2^-, such as between N-bound and chelating. However, the observation that **C** is isolable by applying vacuum and that it forms **D** only upon addition of NO necessarily implies that **C** be an intermediate formed by the reaction of Fe^{2+}-MOF-5 with only 2 equiv of NO. The EXAFS fitting for **C** suggests that the N_xO_y species bound to Fe is η^1 at a distance of 1.98 Å, while the near-edge data confirm that **C** is most likely a ferric species, as corroborated by EPR (Supporting Information Figure S9). Finally, the IR stretch observed in **C** at 1178 cm^{-1} is in the region of N−O bond orders between one and two,[31] while the feature at 868 cm^{-1} is consistent with N−O symmetric stretching modes.[32,33] Together, these data depict **C** as a ferric η^1 hyponitrite radical species.

To further support our vibrational spectroscopy assignments for **C** and **D**, we performed density functional theory calculations on truncated models of Fe^{2+}-MOF-5. Rather than consider the entire lattice, calculations were based on $FeZn_3O(O_2C{-}C_6H_5)_6$ clusters where carbon atoms in the 1 and 4 positions of the benzoates were fixed to simulate geometrical constraints imposed by the MOF (Supporting Information Figures S12−S16). To interrogate **C**, we studied three model compounds with the formula $N_2O_2FeZn_3O(O_2C{-}C_6H_5)_3$ where N_2O_2 is bound either η^1 through a terminal O (ONNO−), η^2 through a side-bound NO group (ONN−O), or η^2 with chelating O atoms (−ONNO−). These coordination modes are shown in Scheme 1. For **D**, we studied two model compounds with the formula $NO_2FeZn_3O(O_2C{-}C_6H_5)_3$ where NO_2 is either bound η^1 through the N atom (−NO_2) or η^2 through chelating O atoms (−ONO−), as also shown in Scheme 1. We also attempted to calculate the isomer where NO_2 is bound η^1 through an O atom, but the calculated geometry converged into chelating coordination. After geometry optimizations, frequency calculations were performed on all compounds to simulate IR spectra and Gibbs free enthalpies at 298.15 K (ΔG). For species **C**, among the N_2O_2 isomers, −ONNO− was predicted to be the most stable, albeit by only 3.59 and 7.08 kcal/mol relative to the ONNO− and ONN−O isomers, respectively. These differences are quite small considering the restrictions imposed on our truncated models. Instead, comparing the calculated parameters with measured observables is more informative. Thus, the Fe−O bond lengths calculated for −ONNO−, 1.88 and 1.89 Å, and for ONN−O, 2.07 Å, are significantly different from that measured by XAS, 1.98 Å. In contrast, closer matches are calculated for the ONNO−isomer, at 2.02 Å. Our calculations predict bond lengths for all isomers of **D** that are longer than that observed, with the −NO_2 isomer in slightly better agreement than the −ONO− isomer, despite the latter being predicted as more stable by 3.63 kcal/mol (see Supporting Information Figures S15 and S16). Despite the chelating isomers being predicted to be more thermodynamically stable, the final geometries resemble end-on coordination modes.

Comparing the calculated frequencies to the observed values aids our identification of **C** and **D**. Among the models

DOI: 10.1021/jacs.5b03761
J. Am. Chem. Soc. 2015, 137, 7495−7501

Table 2. Selected Frequencies of Model Compounds with Assignments[a]

−ONNO−		ONNO−		ONN−O		$-NO_2$		−ONO−	
1430, *1429* (m)	ν_{N-N}	1442, *1419* (s)	ν_{N-O}	1429, *1407* (m)	ν_{N-O}	1417, *1394* (s)	ν_{N-O} (ant)	1237, *1216* (w)	ν_{N-O} (sym)
1426, *1381* (m)	ν_{N-N}	1164, *1140* (m)	ν_{N-O}	1158, *1131* (m)	ν_{N-O}	1267, *1250* (s)	ν_{N-O} (sym)	1168, *1136* (m)	ν_{N-O} (ant)
749, *734* (m)	ν_{O-NN-O}	772, *749* (m)	ν_{N-N}	982, *956* (w)	ν_{N-N}	752, *745* (m)	δ_{ONO}		

[a]Intensities are indicated in parentheses and ^{15}N isotope shifts in italics.

considered for **C**, the structurally similar ONNO− and ONN−O agree better than the chelating −ONNO− (see Table 2). Bands at 1164 and 1158 cm^{-1} for ONNO− and ONN−O, respectively, resemble the observed value of 1178 cm^{-1}, whereas −ONNO− lacks any band in that region. Importantly, our calculations predict that **C** and **D** should exhibit bands between 1400 and 1500 cm^{-1}. However, as shown in Supporting Information Figure S3, that region is dominated by strong MOF-based transitions, which likely mask the expected N_xO_y-based bands. For **D**, the $-NO_2$ isomer has the best match with the experiments. Most tellingly, the alternative −ONO− isomer lacks a band around 700−800 cm^{-1} corresponding to NO_2-based dipole changes. Because this region is devoid of any other bands, the absence of the expected bands for the −ONO− isomer strongly point to $-NO_2$ (i.e., nitro) as the correct assignment for **D**.

To better understand the location of charge and spin density in species **C** and **D**, we analyzed the Natural Atomic Orbitals and Natural Bond Orbitals of −ONNO−, ONNO−, ONN−O, $-NO_2$, and −ONO−. For all model compounds, the Natural Charge and Natural Spin Density on the Fe atom were lower than expected for a high-spin ferric center. As shown in Supporting Information Tables S1−S5, the Natural Charge was calculated to be less than +2 and the Natural Spin Density to be less than 4. Nevertheless, the N and O atoms on the nitrite and hyponitrite ligands possess substantial Natural Spin Density, as do the carboxylate oxygen atoms bound to the Fe. In other words, Fe bears much of the e^- density that would typically be placed on the N_xO_y ligand according to the "X-type" ligand classification method. Another key insight from these analyses is that **C** and **D** are probably best understood through multireference computational methods. Inspecting the Natural Bond Orbitals on Fe reveals each of the d orbitals in the α-manifold to be fully occupied, as would be expected for a high spin ferric center. The β-manifold, however, shows fractional occupation across the d orbitals for all model compounds. Instead of describing the wave function by a single determinant, this fractional occupation indicates that multiple electronic configurations or mixing with low-lying excited states might produce a better agreement with the bond distances determined by EXAFS analysis.

By assigning **C**, we provide the first experimental evidence for an η^1 *monoanionic* hyponitrite radical transition-metal complex. In addition to NO disproportionation,[34−36] transition metal hyponitrite species are invoked as intermediates in NO reduction catalysis for environmental safety[37,38] and in the naturally occurring enzyme NOR.[39] In the few cases where hyponitrite can be isolated, it exists as a closed shell *dianion*. As a dianion, only in select cases it is reported to react further with NO to release N_2O or with acid to produce H_2O.[40,41] In more active catalytic systems, such as NOR, hyponitrite intermediates are also invoked,[42,43] but have not been observed as monoanionic radicals. Indeed, so far $N_2O_2^-$ has only been observed transiently by UV−vis spectroscopy or studied in frozen gas matrices.[44−51]

CONCLUSION

We have shown through site-specific spectroscopy and a host of complementary evidence that Fe^{2+}-MOF-5 promotes nitric oxide disproportionation to release N_2O. This report is a rare example of unusual redox transformations occurring at the metal nodes of a MOF with well characterized changes to their coordination environment and oxidation state. Among the systems known to facilitate nitric oxide disproportionation, Fe^{2+}-MOF-5 is one of the only examples where the mechanism must involve a single iron atom. In homogeneous systems, this mechanistic aspect has been contentious, since bimolecular species can rarely be fully discounted. By elucidating how this reaction occurs at the site-isolated metal sites in a MOF, we hope to learn about mechanistically similar reactions, such as the N−N coupling of 2 equiv of NO in nitric oxide reductase to produce N_2O, and to optimize these materials as unique platforms for N_xO_y reduction catalysis. More generally, our study shows that the metal nodes of MOFs offer a platform for studying reactions of both industrial and biological relevance.

METHODS

In Situ DRIFTS. Measurements were performed on a Bruker Tensor 37 with a mercury cadmium telluride detector cooled to 77 K. Data were collected in the 'MIR_DRIFTS' mode with a 6 mm aperture setting and a KBr beam splitter. The data were averaged over 14 scans between 5000 and 650 cm^{-1} every 15 s. Fully activated Fe-MOF-5 was loaded into a Harrick low temperature environmental chamber and attached to a Harrick Praying Mantis accessory to perform DRIFTS measurements. A measurement was taken of the sample under dynamic vacuum at room temperature, then NO/N_2 was added from a 100 mL Schlenk flask through a Swagelok valve. A spectrum was collected immediately afterward and at regular intervals thereafter.

XAS. Experiments were conducted in the bending magnet beamline of the Materials Research Collaborative Access Team (MRCAT) at the Advanced Photon Source (APS), Argonne National Laboratory. XAS data were acquired at the Fe K-edge (7.112 keV) in transmission step scan mode with photon energies selected using a water-cooled, double-crystal Si(111) monochromator. The monochromator was detuned by approximately 50%, reducing harmonic reflections. The ionization chambers were optimized for the maximum current with linear response (~10^{10} photons detected/s) with 10% absorption (30% N_2 and 70% He) in the incident ion chamber and 70% absorption (90% N_2 and 10% Ar) in the transmission detector.

Each solid standard sample was mixed with boron nitride to a weight ratio of about 4% Fe and the MOF samples were loaded in a glovebox as neat powders. The samples were ground with a mortar and pestle to a uniform size and composition, and then approximately 5−10 mg of the mixture was pressed into a cylindrical sample holder consisting of six wells with a radius of 4.0 mm, forming a self-supporting wafer. An Fe foil spectrum was acquired simultaneously with each measurement for energy calibration. The sample holder was placed in a quartz tube (1 in. o.d., 10 in. length) sealed with Kapton windows by two Ultra-Torr fittings and then used for transmission mode measurement.

The edge energy of the X-ray absorption near edge structure (XANES) spectrum was determined from the inflection point in the edge, i.e., the maximum in the first derivative of the XANES spectrum.

DOI: 10.1021/jacs.5b03761
J. Am. Chem. Soc. 2015, 137, 7495−7501

The pre-edge energy was determined from the maximum of the pre-edge peak. Experimental phase shift and back scattering amplitude were used to fit the EXAFS data. Fe−O phase shift and back scattering amplitude were obtained from reference compounds: $Fe(acac)_3$ (6 Fe−O at 1.91 Å). Background removal and normalization procedures were carried out using the Athena software package using standard methods. Standard procedures based on WinXAS 3.2 software were used to extract the extended X-ray absorption fine structure (EXAFS) data. The coordination parameters were obtained by a least-square fit in R-space of the nearest neighbor, k^2-weighted Fourier transform data.

■ ASSOCIATED CONTENT

Supporting Information

Experimental and computational details. Magnetic susceptibility, RGA-MS, PXRD and N_2 isotherm data. Diffuse reflectance UV−vis, EPR, ^{57}Fe Mössbauer, and additional DRIFTS spectra. Geometry-optimized structures. The Supporting Information is available free of charge on the ACS Publications website at DOI: 10.1021/jacs.5b03761.

■ AUTHOR INFORMATION

Corresponding Author

*mdinca@mit.edu

Funding

Partial funding for J.T.M. was provided by Chemical Sciences, Geosciences and Biosciences Division, U.S. Department of Energy, under contract DE-AC0-06CH11357.

Notes

The authors declare no competing financial interest.

■ ACKNOWLEDGMENTS

This work was supported by the National Science Foundation, under Award DMR-1452612. MD thanks the Sloan Foundation, the Research Corporation for Science Advancement, and 3M for nontenured faculty awards. C.K.B. acknowledges partial support from the NSF through a Graduate Research Fellowship through Grant 1122374. We thank Matthew Nava for assistance with NBO analysis. MRCAT operations are supported by the Department of Energy and the MRCAT member institutions. This research used resources of the Advanced Photon Source, a U.S. Department of Energy (DOE) Office of Science User Facility operated for the DOE Office of Science by Argonne National Laboratory under Contract No. DE-AC02-06CH11357. Part of this work was performed at the National High Magnetic Laboratory (NHMFL), which is supported by the NSF (DMR-1157490) and the State of Florida. S.A.S. would also like to acknowledge the NHMFL Jack E. Crow Postdoctoral Fellowship. The Mössbauer instrument was purchased using the NHMFL User Collaboration Grant Program (UCGP-5064) awarded to Dr. Andrzej Ozarowski.

■ REFERENCES

(1) Lelieveld, J.; Crutzen, P. J. *Science* **1994**, *264*, 1759.
(2) Liu, F.; He, H.; Xie, L. *ChemCatChem* **2013**, *5*, 3760.
(3) Long, J.; Zhang, Z.; Ding, Z.; Ruan, R.; Li, Z.; Wang, X. *J. Phys. Chem. C* **2010**, *114*, 15713.
(4) Ignarro, L. J. *Nitric Oxide: Biology and Pathobiology*; 2nd ed.; Academic Press: San Diego, CA, 2009.
(5) Yu, A. E.; Hu, S.; Spiro, T. G.; Burstyn, J. N. *J. Am. Chem. Soc.* **1994**, *116*, 4117.
(6) Xiao, D. J.; Bloch, E. D.; Mason, J. A.; Queen, W. L.; Hudson, M. R.; Planas, N.; Borycz, J.; Dzubak, A. L.; Verma, P.; Lee, K.; Bonino, F.; Crocellà, V.; Yano, J.; Bordiga, S.; Truhlar, D. G.; Gagliardi, L.; Brown, C. M.; Long, J. R. *Nat. Chem.* **2014**, *6*, 590.
(7) Denysenko, D.; Grzywa, M.; Jelic, J.; Reuter, K.; Volkmer, D. *Angew. Chem., Int. Ed.* **2014**, *53*, 5832.
(8) Cozzolino, A. F.; Brozek, C. K.; Palmer, R. D.; Yano, J.; Li, M.; Dincă, M. *J. Am. Chem. Soc.* **2014**, *136*, 3334.
(9) Brozek, C. K.; Dincă, M. *J. Am. Chem. Soc.* **2013**, *135*, 12886.
(10) Bloch, E. D.; Murray, L. J.; Queen, W. L.; Chavan, S.; Maximoff, S. N.; Bigi, J. P.; Krishna, R.; Peterson, V. K.; Grandjean, F.; Long, G. J.; Smit, B.; Bordiga, S.; Brown, C. M.; Long, J. R. *J. Am. Chem. Soc.* **2011**, *133*, 14814.
(11) Bloch, E. D.; Queen, W. L.; Chavan, S.; Wheatley, P. S.; Zadrozny, J. M.; Morris, R.; Brown, C. M.; Lamberti, C.; Bordiga, S.; Long, J. R. *J. Am. Chem. Soc.* **2015**, *137*, 3466.
(12) Collman, J. P.; Yang, Y.; Dey, A.; Decréau, R. A.; Ghosh, S.; Ohta, T.; Solomon, E. I. *Proc. Natl. Acad. Sci. U.S.A.* **2008**, *105*, 15660.
(13) Collman, J. P.; Dey, A.; Yang, Y.; Decréau, R. A.; Ohta, T.; Solomon, E. I. *J. Am. Chem. Soc.* **2008**, *130*, 16498.
(14) Wasser, I. M.; De Vries, S.; Moënne-Loccoz, P.; Schröder, I.; Karlin, K. D. *Chem. Rev.* **2002**, *102*, 1201.
(15) Moënne-Loccoz, P. *Nat. Prod. Rep.* **2007**, *24*, 610.
(16) Varotsis, C.; Ohta, T.; Kitagawa, T.; Soulimane, T.; Pinakoulaki, E. *Angew. Chem., Int. Ed.* **2007**, *46*, 2210.
(17) Tosha, T.; Shiro, Y. *IUBMB Life* **2013**, *65*, 217.
(18) Kaye, S. S.; Dailly, A.; Yaghi, O. M.; Long, J. R. *J. Am. Chem. Soc.* **2007**, *129*, 14176.
(19) Webb, P. A.; Orr, C. *Analytical Methods in Fine Particle Technology*; Micromeritics Instrument Corporation: Norcross, GA, 1997.
(20) Gütlich, P.; Bill, E.; Trautwein, A. X. *Mössbauer Spectroscopy and Transition Metal Chemistry Fundamentals and Applications*; Springer-Verlag: Berlin, Heidelberg, 2011.
(21) Bou-Abdallah, F.; Chasteen, N. D. *J. Biol. Inorg. Chem.* **2008**, *13*, 15.
(22) Martirosyan, G. G.; Azizyan, A. S.; Kurtikyan, T. S.; Ford, P. C. *Inorg. Chem.* **2006**, *45*, 4079.
(23) Tsai, F.-T.; Lee, Y.-C.; Chiang, M.-H.; Liaw, W.-F. *Inorg. Chem.* **2013**, *52*, 464.
(24) Tsai, F. Te; Kuo, T. S.; Liaw, W. F. *J. Am. Chem. Soc.* **2009**, *131*, 3426.
(25) Weber, B.; Käpplinger, I.; Görls, H.; Jäger, E.-G. *Eur. J. Inorg. Chem.* **2005**, *2005*, 2794.
(26) Villar-Acevedo, G.; Nam, E.; Fitch, S.; Benedict, J.; Freudenthal, J.; Kaminsky, W.; Kovacs, J. A. *J. Am. Chem. Soc.* **2011**, *133*, 1419.
(27) Ellison, M. K.; Ellison, M. K.; Schulz, C. E.; Schulz, C. E.; Scheidt, W. R.; Scheidt, W. R. *Polyhedron* **1999**, *38*, 100.
(28) Patra, A. K.; Rose, M. J.; Olmstead, M. M.; Mascharak, P. K. *J. Am. Chem. Soc.* **2004**, *126*, 4780.
(29) Tsai, F.-T.; Chen, P.-L.; Liaw, W.-F. *J. Am. Chem. Soc.* **2010**, *132*, 5290.
(30) Arulsamy, N.; Bohle, D. S.; Hansert, B.; Powell, A. K.; Thomson, A. J.; Wocaldo, S. *Inorg. Chem.* **1998**, *37*, 746.
(31) Nakamoto, K. *Infrared and Raman Spectra of Inorganic and Coordination Compounds*; 6th ed.; Wiley: Hoboken, NJ, 2009.
(32) Villalba, M. E. C.; Navaza, A.; Güida, J. A.; Varetti, E. L.; Aymonino, P. J. *Inorg. Chim. Acta* **2006**, *359*, 707.
(33) Lippincott, R. *Chem. Commun.* **1946**, *987*, 1820.
(34) Ruggiero, C. E.; Carrier, S. M.; Tolman, W. B. *Angew. Chem., Int. Ed. Engl.* **1994**, *33*, 895.
(35) Franz, K. J.; Lippard, S. J. *J. Am. Chem. Soc.* **1999**, *121*, 10504.
(36) Franz, K. J.; Lippard, S. J. *J. Am. Chem. Soc.* **1998**, *120*, 9034.
(37) Macneil, J. H.; Berseth, P. A.; Bruner, E. L.; Perkins, T. L.; Wadia, Y.; Westwood, G.; Trogler, W. C. *J. Am. Chem. Soc.* **1997**, *119*, 1668.
(38) Ford, P. C.; Lorkovic, I. M. *Chem. Rev.* **2002**, *102*, 993.
(39) Hino, T.; Matsumoto, Y.; Nagano, S.; Sugimoto, H.; Fukumori, Y.; Murata, T.; Iwata, S.; Shiro, Y. *Science* **2010**, *330*, 1666.
(40) Gans, P. *J. Chem. Soc. A* **1967**, 943.

DOI: 10.1021/jacs.5b03761
J. Am. Chem. Soc. 2015, 137, 7495−7501

(41) Wright, A. M.; Wu, G.; Hayton, T. W. *J. Am. Chem. Soc.* **2012**, *134*, 9930.
(42) Berto, T. C.; Xu, N.; Lee, S. R.; McNeil, A. J.; Alp, E. E.; Zhao, J.; Richter-Addo, G. B.; Lehnert, N. *Inorg. Chem.* **2014**, *53*, 6398.
(43) Caranto, J. D.; Weitz, A.; Hendrich, M. P.; Kurtz, D. M. *J. Am. Chem. Soc.* **2014**, *136*, 7981.
(44) Poskrebyshev, G. A.; Shafirovich, V.; Lymar, S. V. *J. Phys. Chem. A* **2008**, *112*, 8295.
(45) Forney, D.; Jacox, M. E.; Thompson, W. E. *J. Mol. Spectrosc.* **1992**, *153*, 680.
(46) Li, R.; Continetti, R. E. *J. Phys. Chem. A* **2002**, *106*, 1183.
(47) Andrews, L.; Citra, A. *Chem. Rev.* **2002**, *102*, 885.
(48) Lymar, S. V.; Shafirovich, V.; Poskrebyshev, G. A. *Inorg. Chem.* **2005**, *44*, 5212.
(49) Andrews, L.; Zhou, M. *J. Chem. Phys.* **1999**, *111*, 6036.
(50) Andrews, L.; Zhou, M.; Willson, S. P.; Kushto, G. P.; Snis, A.; Panas, I. *J. Chem. Phys.* **1998**, *109*, 177.
(51) Valiev, M.; Lymar, S. V. *J. Phys. Chem. A* **2011**, *115*, 12004.

DOI: 10.1021/jacs.5b03761
J. Am. Chem. Soc. 2015, 137, 7495−7501